Contribution from the Departments of Chemistry and Physics,
Iowa State University, Ames, Iowa 50011

Two Extended Metal Chain Compounds, Y_4I_5C and $Y_6I_7C_2$. Synthesis, Structure, Properties, and Bonding

Susan M. Kauzlarich,[1a] Timothy Hughbanks,[2] John D. Corbett,* Peter Klavins,[1b] and Robert N. Shelton[1b]

Received December 29, 1987

The title phases are obtained in high yield from the reactions of stoichiometric quantities of Y, YI_3, and graphite at 850–950 °C in welded Nb containers. The crystal structures of the two phases determined by standard X-ray diffraction means are related to those published for Er_4I_5 and Er_6I_7 ($C2/m$, $Z = 2$, $a = 18.479$ (6) and 21.557 (8) Å, $b = 3.947$ (1) and 3.909 (1) Å, $c = 8.472$ (3) and 12.374 (6) Å, $\beta = 103.22$ (4) and 123.55 (3)°, $R/R_w = 4.6/5.4$ and 3.2/3.7% for Y_4I_5C and $Y_6I_7C_2$, respectively). The two compounds contain infinite single and double chains of carbon-centered yttrium octahedra, respectively, condensed by edge-sharing and sheathed by edge-bridging iodine atoms together with square-planar iodine atoms that bridge between chains. Extended Hückel MO band calculations were carried out for the empty and the carbon-centered compounds in both structures. Metal-based bands near E_F in the empty chains exhibit characteristic strong interactions with carbon valence orbitals that generate low-lying valence bands. E_F in both cases falls within a broad, metal-based conduction band. Resistivity and magnetic susceptibility measurements on $Y_6I_7C_2$ support the predicted metallic character.

Introduction

The rare-earth-metal iodides form a variety of highly reduced phases that contain metal clusters. The basic framework in nearly all of these compounds consists of either discrete or condensed edge-sharing R_6I_{12}-type octahedral clusters (R = rare-earth metal). The most common structure, the rhombohedral $R(R_6I_{12}Z)$ type, has been recognized for R = Sc, Y, La, Pr, Gd, Tb, and Er and probably can be found for other elements in the series. All the clusters in these are found to be centered by a strongly bound interstitial entity Z such as B, C, N, C_2,[3-6] or, more recently, a transition metal in the series Mn–Ni.[7]

Similar iodide clusters condensed into infinite chains have been reported for the compositions Er_4I_5, Er_6I_7, and Er_7I_{10},[8,9] and the existence of Gd_4I_5C, $Gd_6I_7C_2$, and $Gd_6Br_7C_2$ has also been cited.[6] The only known exceptions to the occupancy of all rare-earth-metal octahedra in these compounds by an interstitial atom appear to be in half of the chains in the novel $Y_{10}I_{13}O_2$[10] and in the related sesquihalides that are known for the lighter halides of some of these metals, Y_2Cl_3 and Y_2Br_3 among them.[11] Finally, the further condensation of cluster iodides into double-metal sheets has been found for GdIH,[12] and comparable phases can probably be formed with several other rare-earth elements.

In our synthetic and property studies on Y_2Cl_2C and related systems,[10] we have also pursued the possibility of preparing other ternary yttrium chloride or iodide phases that contain nonmetallic interstitial elements. The preparation of two acicular products in the Y–I–C system has to date been the most successful, and the X-ray diffraction studies reported here show these to be Y_4I_5C and $Y_6I_7C_2$, isostructural with the binary erbium phases noted above. The compounds have been characterized further by means of magnetic susceptibility and resistivity measurements. Since results of tight-binding calculations for the empty Er_4I_5 and Er_6I_7 chain structures have been briefly described,[13] it was considered worthwhile to carry out extended Hückel calculations on the analogous yttrium iodides with and without carbon both to clarify the role of a nonmetal and to compare the results with the metal-like conductivity measured for $Y_6I_7C_2$.

Experimental Section

Syntheses. The high-purity Y metal (Ames Lab) was arc-melted, cold rolled to ~0.4-mm thick strips, and cut into small pieces (~3 × 3 mm). Yttrium triiodide was prepared by reaction of the elements in a sealed fused silica apparatus as before.[14] Yttrium pieces contained in an internal tungsten crucible were heated at 850 °C for 3 days under iodine from a reservoir maintained at 150 °C. The crude light gray product was sublimed three times under high vacuum within a tantalum apparatus to give very pure YI_3.

Typical vacuum and drybox techniques were used whenever the materials were not sealed in Pyrex storage or niobium reaction containers. Single-phase $Y_6I_7C_2$ was prepared in ~100% yield at 950 °C by reaction of excess Y with stoichiometric quantities of YI_3 (~200 mg) and graphite. The silica-jacketed container was rapidly cooled afterwards in air. Reaction periods as short as 1 week provided high yields, but crystal growth was improved by allowing 2–3 weeks, after which black needle crystals as long as 1 cm could be found. Although no temperature gradient was purposely imposed, enough of a gradient evidently occurred naturally along the 2-in. niobium container, and the tightly adhering crystals were found growing on one end of the Y strip. Dark red Y_4I_5C was produced as the major product (~70%) from a similar reaction of excess Y strips with stoichiometric amounts of YI_3 (~200 mg) and C at 850 °C. The other products were $Y_6I_7C_2$ and a small amount of unreacted YI_3. In connection with the identity of the interstitial atom, it is important to note that elimination of the graphite reactant alone from the reactions yields only Y and YI_3 and, on occasion, traces of small black needle crystals that probably derive from carbon impurities.

Suitable needle crystals of Y_4I_5C and $Y_6I_7C_2$ were sealed in thin-walled glass capillaries in a drybox. The structure types were initially identified by Weissenberg photographs (zero and first layer). The crystals appeared to have structures similar to those reported for Er_4I_5[8] and Er_6I_7[9] based on the observed lattice constants and *C*-centering, and this model was found to account well for all lines in the Guinier patterns with respect to both position and intensity. Both phases gave good Weissenberg patterns with little streaking or diffuse scattering on the films, and this was especially true for $Y_6I_7C_2$. Powder patterns (monochromatic Cu $K\alpha_1$, $\lambda = 1.540\,562$ Å) were obtained with an Enraf-Nonius (FR-552) Guinier camera. Samples were ground in a drybox, mixed with a little NBS silicon powder as an internal standard, and mounted between two pieces of cellophane tape to protect them from

* To whom correspondence should be addressed at the Department of Chemistry, Iowa State University.

(1) Present address: (a) Department of Chemistry, University of California, Davis, CA 95616. (b) Department of Physics, University of California, Davis, CA 95616.
(2) Present address: Department of Chemistry, Texas A&M University, College Station, TX 77843.
(3) Dudis, D. S.; Corbett, J. D. *Inorg. Chem.* **1987**, *26*, 1933.
(4) Dudis, D. S.; Corbett, J. D.; Hwu, S.-J. *Inorg. Chem.* **1986**, *25*, 3434.
(5) Simon, A.; Warkentin, E. *Z. Anorg. Allg. Chem.* **1983**, *497*, 79.
(6) Simon, A. *J. Solid State Chem.* **1985**, *57*, 2.
(7) (a) Hughbanks, T.; Rosenthal, G.; Corbett, J. D. *J. Am. Chem. Soc.* **1986**, *108*, 8289. (b) Hughbanks, T.; Rosenthal, G.; Corbett, J. D. *J. Am. Chem. Soc.* **1988**, *110*, 1511. (c) Hughbanks, T.; Corbett, J. D. *Inorg. Chem.*, in press.
(8) Berroth, K.; Simon, A. *J. Less-Common Met.* **1980**, *76*, 41.
(9) Berroth, K.; Mattausch, H.; Simon, A. *Z. Naturforsch, Sect. B: Anorg. Chem., Org. Chem.* **1980**, *356*, 626.
(10) Kauzlarich, S. M.; Corbett, J. D., unpublished research.
(11) Mattausch, H.; Hendricks, J. G.; Eger, R.; Corbett, J. D.; Simon, A. *Inorg. Chem.* **1980**, *19*, 2128.
(12) Mattausch, H.; Schramm, W.; Eger, R.; Simon, A. *Z. Anorg. Allg. Chem.* **1985**, *530*, 43.
(13) Bullett, D. W. *Inorg. Chem.* **1985**, *24*, 3319.
(14) Corbett, J. D. *Inorg. Synth.* **1983**, *22*, 31.

0020-1669/88/1327-1791$01.50/0

Table I. Crystal and Refinement Data for Y_4I_5C and $Y_6I_7C_2$

	Y_4I_5C	$Y_6I_7C_2$
space group	$C2/m$	$C2/m$
Z	2	2
cell params[a]		
a, Å	18.479 (6)	21.557 (8)
b, Å	3.947 (1)	3.9093 (9)
c, Å	8.472 (3)	12.374 (6)
β, deg	103.22 (4)	123.55 (3)
V, Å^3	601.6 (3)	869.0 (5)
cryst dimens, mm	0.5 × 0.025 × 0.02	0.5 × 0.05 × 0.03
octants measd	hkl, $\bar{h}kl$, $\bar{h}k\bar{l}$, $hk\bar{l}$	hkl, $\bar{h}kl$, $\bar{h}l\bar{l}$, $hk\bar{l}$
2θ(max), deg	55	55
no. of reflcns		
measd	1735	2867
obsd[b]	1400	1763
indep	605	836
R(av), %	0.054	0.023
extinct coeff × 10^{-4}		0.15 (3)
abs coeff μ, cm^{-1} (Mo Kα)	319	322
transmissn coeff range	0.18–0.42	0.12–0.35
R,[c] %	4.6	3.2
R_w,[d] %	5.4	3.7

[a] Guinier powder data. [b] $F_{obsd} \geq 3\sigma_F$ and $I_{obsd} > 3\sigma_I$. [c] $r = \sum(|F_o| - |F_c|)/\sum|F_o|$. [d] $R_w = [\sum w(|F_o| - |F_c|)^2/\sum w|F_o|^2]^{1/2}$, $w = \sigma_F^{-2}$.

moisture and oxygen. The samples were thereafter maintained in a forepump vacuum within the camera.

Low-temperature powder diffraction patterns were obtained for $Y_6I_7C_2$ by using an Air Products closed-cycle refrigerator mounted on a Rigaku powder diffractometer. X-ray scans were taken in the range $20 \leq 2\theta \leq 60°$ at ~293 K and at ~25 K at scan rates of 0.01 deg s^{-1}. No phase transitions were evident over this range.

Crystallography. Diffraction data for Y_4I_5C and $Y_6I_7C_2$ were collected at room temperature on Datex (ω scan) and Syntex $P2_1$ (ω–2ω) diffractometers, respectively, utilizing monochromated Mo Kα radiation. Crystallographic data are summarized in Table I. There was no indication of intensity decay with time for either crystal. The data were corrected for absorption empirically with the aid of two ψ scans each as well as for Lorentz and polarization effects. Refinements started with the heavy-atom positions reported for the erbium iodides and proceeded uneventfully. Fourier maps calculated after anisotropic thermal parameters had been introduced for both atoms clearly revealed the carbon atoms in the center of the metal octahedra in both phases.

Simultaneous occupancy refinements of all atoms in Y_4I_5C except Y1 revealed no problems, the results deviating no more than 2% (2σ) from unity for heavy atoms, 8% (1σ) for carbon. The final Fourier electron density map for Y_4I_5C exhibited peaks corresponding to ~7 e/Å^3 about 2 Å away from I1 and I2, but the difference Fourier map was flat to less than ±1 e/Å^3. The extra features in the former lay largely in a density streak through the iodines and parallel to $\vec{c}$. This behavior appears to be a clear manifestation of truncation errors in the data set; in support of this, the reflection intensities were observed to remain relatively strong even at $2\theta = 50°$.

The refinement of $Y_6I_7C_2$ likewise indicated no significant deviations from full occupancy of all positions. The final Fourier map contained residual peaks of ~2.6 e/Å^3 displaced along $\vec{a}$ from the iodine atoms, but the difference map was flat to ±0.6 e/Å^3, again an evident result of an incomplete data set from a well-diffracting crystal. In both cases the missing data evidently come principally from diffraction by planes more or less parallel to the sheets of chains that are strongly bonded together by four-coordinate iodine (see below).

Programs utilized and the sources of scattering factors, including imaginary components, were as referenced earlier.[15]

Resistivity Measurements. Standard four-probe ac resistivity measurements were made along the needle (b) axis at low frequency (~25 Hz) on single crystals of $Y_6I_7C_2$ that had typical dimensions of 0.2 × 0.1 × 5.0 mm. Because of the extreme air sensitivity of both $Y_6I_7C_2$ and Y_4I_5C, the crystals were handled only in a nitrogen-filled drybox that had a water level of a few ppm. The crystals were mounted on a fritted glass disk and were first held in place by small drops of silver epoxy to which 0.05-mm diameter Pt wires were attached. Large phase shifts in the signal were observed, indicating poor contacts between the sample and Pt leads. After many attempts it was concluded that the crystals reacted with both commercial silver epoxy and silver paint. Gold sputtering was attempted once but the extreme air sensitivity of the crystals made this impractical. Finally, satisfactory measurements were obtained using pressed In contacts between the crystal and the Pt wires. The four leads so attached were soldered to terminal posts of the sample holder. The sample holder could be closed in the drybox and transferred to the cryostat for measurement without exposure to air. No phase shifts were observed in the signal during the measurements.

Magnetic Susceptibilities. Measurements were made by using a Quantum Design SQUID magnetometer over the temperature range 2–340 K. Ground crystals of the phases were placed into a thin-walled fused silica holder and sealed under vacuum to prevent reaction with air.

Extended Hückel Calculations. Tight-binding, band structure calculations were carried out on one-dimensional chains $^1_\infty[Y_6I_{10}C_2^{3-}]$, $^1_\infty[Y_6I_{10}^{3-}]$, $^1_\infty[Y_4I_8C^{3-}]$, and $^1_\infty[Y_4I_8^{3-}]$ in order to clarify aspects of the metal–metal and metal–carbon bonding in these materials. Structural parameters used in the calculations were taken from the X-ray refinements except that positional data for the single chain in Y_4I_5 were slightly modified to incorporate the two pseudo mirror planes that lie along the chain axis, σ_{xy}, which contains carbon and the shared Y–Y edges, and σ_{xz}, the carbon and apex metal atoms. This was done merely to facilitate subsequent symmetry analysis; minor deviations from mirror symmetry will lead to physically insignificant but inconvenient avoided crossings in the bands.

Input parameters for yttrium (H_{ii} values) were obtained from our previous unpublished charge-iterative calculation for YB_4. Subsequent charge-iterative calculations on chemically more similar compounds have shown us that the value used for the 4d orbitals ($H_{dd} = -8.32$ eV) is probably about 1 eV too deep in energy. However, since changing these values would only serve to widen the iodine p–yttrium d band gap by a comparable amount without substantially altering the d bands themselves, the calculations were not repeated. The full set of parameters is supplied in the supplementary material.

Table II. Positional Parameters for Y_4I_5C and $Y_6I_7C_2$[a]

atom	x	z
	Y_4I_5C	
Y1	0.00047 (8)	0.8083 (2)
Y2	0.63414 (8)	0.0678 (2)
I1	0.16718 (5)	0.3476 (1)
I2	0.17117 (5)	0.8198 (1)
I3	0.5	0.5
C	0.5	0
	$Y_6I_7C_2$	
Y1	0.76744 (6)	0.8256 (1)
Y2	0.31050 (6)	0.6312 (1)
Y3	0.13689 (6)	0.5582 (1)
I1	0.39415 (4)	0.94216 (8)
I2	0.16050 (5)	0.83421 (9)
I3	0.05427 (4)	0.27048 (8)
I4	0.5	0.5
C	0.7193 (5)	0.6018 (12)

[a] $y = 0$ for all atoms, space group $C2/m$.

Results and Discussion

Crystal Structures. The synthesis of well-formed crystals of Y_4I_5C and $Y_6I_7C_2$ in high yield again demonstrates the essential character of an interstitial atom, carbon in this instance, in stabilizing such phases. The product mixture obtained was largely dependent only on stoichiometric proportions of the $Y/YI_3/C$ reactants, while omission of carbon from the reactants provides no reduced phases in significant amounts, in agreement with published phase studies.[16] Considering the pseudo-one-dimensional character of the refined structures for the two new phases, the quality of the crystals studied is noteworthy, namely, in the absence of appreciable diffuse scattering, in their strong diffraction at high angles, and in the character of the refined thermal ellipsoids, to the extent that the last reflect the absence of substantial disorder or other defects. The refined positional parameters obtained for Y_4I_5C and $Y_6I_7C_2$ are reported in Table II, while the thermal parameters as well as observed and calculated structure factors are available as supplementary material.

Figures 1 and 2 view the structures of Y_4I_5C and $Y_6I_7C_2$ down the short (~3.9 Å) b axis, along which all atoms lie in layers at

(15) Hwu, S.-J.; Corbett, J. D.; Poeppelmeier, K. P. *J. Solid State Chem.* **1985**, *57*, 43.

(16) Corbett, J. D.; Pollard, D. L.; Mee, J. E. *Inorg. Chem.* **1966**, *5*, 761.

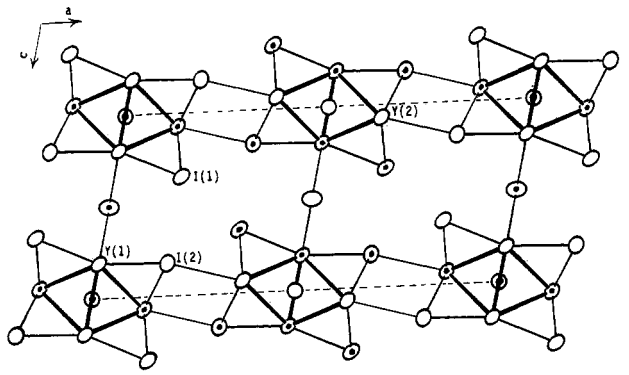

Figure 1. Projection of the structure of Y_4I_5C along the short b axis. The yttrium atoms that comprise the clusters are interconnected by the heavier lines with carbon centered within these. The open ellipsoids are at $y = 0$; the dotted ones are at $y = {}^1/_2$ (90% probability thermal ellipsoids).

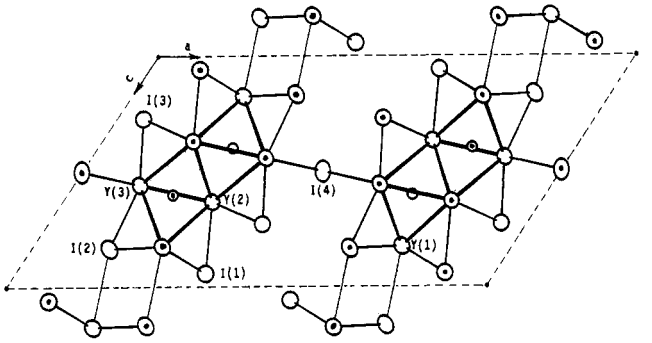

Figure 2. [010] projection of the structure of $Y_6I_7C_2$. The yttrium atoms in the clusters are interconnected by the heavier lines with carbon centered within these figures. The open spheres are $y = 0$; the dotted ones are at $y = {}^1/_2$ (90% thermal ellipsoids).

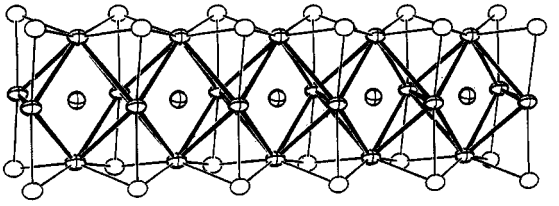

Figure 3. Portion of the infinite chain of edge-sharing yttrium octahedra in Y_4I_5C. Iodine atoms are the open ellipsoids. The repeat distance along the chain is 22% longer than the shared edge (90% thermal ellipsoids).

either $y = 0$ or ${}^1/_2$ (dotted ellipsoids). The arrangement of yttrium atoms is seen to generate nominal metal octahedra that share trans edges to form infinite chains, while iodine atoms bridge all exposed edges of these polyhedra. The three-dimensional structures can be generated easily if the cluster chains are in both cases joined first into sheets by four-coordinate iodine in a planar array (d(Y–I) = 3.27 Å), and then at the cluster vertices in the third dimensions by longer interchain bridges (3.50–3.59 Å) that bond to edge-bridging iodines in other chains. Table III provides important bond distances and angles in both compounds.

Y_4I_5C. Figure 1 clearly shows the interconnection of parallel chains by I3 atoms at the waist of the metal octahedra (Y1) that yields sheets of chains centered in the (200) planes. These sheets are then linked by a mutually complementary bonding of I2 atoms in one chain to Y2 vertices in the other, roughly along $\vec{a}$. A view of a portion of an individual chain, Figure 3, illustrates the result of condensation of Y_6I_{12}-type clusters so that iodine atoms still bridge all edges of the metal framework. (The side edges are also bridged by the interchain I3.) The metal "octahedra" are characteristically elongated, 3.95 Å along the repeat versus a short 3.25 Å in the shared edge, although the longer separation might in these compounds be viewed as a virtual necessity in order to accommodate large iodine atoms with the same 3.95 Å repeat

Table III. Distances (Å) and Angles (deg) for Y_4I_5C and $Y_6I_7C_2$[a]

	Y_4I_5C	$Y_6I_7C_2$
	Distances	
Y1–Y1	3.248 (3)	
Y1–Y2	3.512 (2)	3.597 (2)
Y1–Y2	3.513 (2)	
Y1–Y3		3.521 (2)
Y2–Y2		3.437 (3)
Y2–Y3		3.329 (2)
Y2–Y3′		3.679 (2)
Y1–I1	3.074 (2)	3.001 (1)
Y1–I3	3.270 (1)	
Y1–I2	3.130 (2)	3.069 (1)
Y1–I2[b]		3.592 (3)
Y2–I1	3.036 (1)	3.222 (2)
Y2–I2	3.070 (1)	
Y2–I2[b]	3.503 (2)	
Y2–I3		3.143 (1)
Y3–I3		2.973 (3)
Y3–I2		3.163 (2)
Y3–I4[b]		3.271 (1)
I1–I1	4.039 (2)[c]	3.957 (2)[c]
I1–I2	3.980 (2)[c]	
I1–I2	4.090 (1)	4.058 (2)
I1–I3		3.900 (2)
		4.091 (2)[c]
I2–I3		4.060 (2)
Y1–C	2.556 (1)	2.360 (12)
Y2–C	2.410 (2)	2.585 (12)
Y2–C		2.651 (7)
Y3–C		2.492 (6)
	Angles	
Y1–Y1–Y2	55.82 (2)	56.28 (2)
Y1–Y1–Y2	62.45 (5)	57.08 (2)
Y2–Y1–Y2	68.35 (4)	65.84 (4)
Y2–Y1–Y3	55.76 (4)	
Y1–Y2–Y3	60.98 (4)	
Y3–Y1–Y3	67.43 (5)	
Y2–Y2–Y3	57.91 (2)	
Y2–Y3–Y2	58.47 (4)	
Y1–I1–Y2	70.17 (4)	70.50 (4)
Y1–I2–Y2	69.01 (4)	
Y2–I2–Y2′	80.00 (5)	
Y2–I1–Y2′	81.08 (4)	
Y1–I2–Y3		68.79 (4)
Y1–I2–Y1′		79.13 (4)
Y1–I1–Y1′		81.28 (5)
Y2–I3–Y3		73.92 (4)
Y1–I3–Y1′	74.22 (3)	
Y3–I4–Y3′		73.39 (4)
Y1–C–Y1′	78.91 (5)	
Y2–C–Y3		80.63 (5)
Y2–C–Y2		82.0 (3)
Y1–C–Y3		93.0 (3)
Y1–C–Y2		91.5 (4)

[a] All atoms also have two like neighbors at $\pm c$, 3.947(1) Å in Y_4I_5C; 3.909 (1) Å in $Y_6I_7C_2$. [b] Interchain bridging. [c] Between strings of clusters that are joined by four-coordinate iodine.

along the chain. Other iodine–iodine contacts in the structure range down to 3.98 Å between I2 and I1 in adjoining chains along $\vec{c}$. The pairs of long (3.50 Å) I2–Y2 interchain bridges along $\vec{a}$ do not appear to result from especially tight I–I contacts between neighboring atoms, which are 4.09 Å or larger. We are inclined instead to view these as reflections of distinctly weaker covalent bonding at the metal vertices. The Y–I bonding distances observed about the chain parallel the coordination numbers of the non-metal, which range from 3.04–3.07 Å for two-coordinate I1 up to 3.27 Å for the bridging, four-coordinate I3; of course, the latter presumably utilizes intrinsically different bonding orbitals on the metal chain too.

The elongation of the octahedra and nature of the interchain connectivity by I3 are more clearly shown in Figure 4 in a view along [100], the edge-bridging I1 and I2 atoms being omitted for

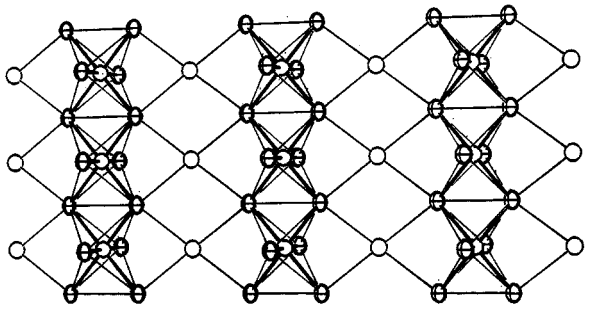

Figure 4. Approximately [100] view of the $^{1}_{\infty}[Y_{4/2}Y_2C]$ chains in Y_4I_5C together with the interconnecting I3. Heavier lines emphasize the Y–C bonding. The edge-bridging I1 and I2 have been omitted for clarity.

clarity. The rectangular rather than square-planar coordination about I3 presumably reflects the short I1–I2 contacts between chains, 3.98 Å, noted above.

Although lines have not been included in all of the figures to represent Y–C bonding interactions, these are certainly strong (see below). The environment about carbon is somewhat distorted, being 2.410 Å to the four waist metal atoms (Y1) and 2.556 Å to the two vertices of the "octahedron". The distribution may reflect an overly small size of the interstitial relative to iodine. The average Y–C value, 2.46 Å, corresponds to an effective carbon radius of 1.42 Å when the six-coordinate crystal radius[17] is applied for yttrium. This is *exactly* the value similarly deduced from a large number of zirconium chloride carbide clusters,[18] and it is also close to the 1.40 and 1.43 Å values likewise obtained from data for $Sc_7I_{12}C$[4] and $Sc_7Cl_{10}C_2$.[15]

The present structure can be seen to be closely related to that in Sc_5Cl_8Z (Z = B, N).[19] The latter is stoichiometrically $ScCl_3{\cdot}Sc_4Cl_5Z$, the additional $ScCl_3$ appearing as parallel, infinite chains of edge-sharing $Sc_4Cl_{4/2}Cl_2$ octahedra in which all of the chlorine atoms are also bonded to terminal positions on the Sc_4Cl_5Z chains. The structure as depicted in Figure 1 can be converted to that of Sc_5Cl_8 directly and simply by rotation of all chains clockwise by ~35°, expansion of the structure, and replacement of the center bridging I3, etc. by these $ScCl_{4/2}Cl_2$ chains. The last are positioned so that the chlorine atoms therein bond not only to what are here two Y1 atoms but also to the inward facing Y2 vertices in cluster chains located at 0,0,1 and 1,1,1, and so on.

The Er_4I_5 model structure that provided the initial heavy-atom positions for the refinement of Y_4I_5C has to date been reported only for iodides. The instability of the R_5I_8C alternative may be associated with the relatively long bonds to iodine at the Y2 (Sc3) vertices. The "Er_4I_5" studied earlier presumably also contained a third element within the metal octahedra. Its synthesis in the pseudo-binary Er–ErI_3 system characteristically provided only trace amounts under what were described as seemingly "alchemistic" conditions.[8] A residual equivalent to ~0.1 iodine was found in the center of the erbium octahedra, but the crystallographic effort was seriously handicapped by multiple or twinned crystals. However, the dimensions obtained for Er_4I_5 strongly suggest that the phase studied was not the carbide or one with a similarly sized impurity. Although nearly all of the Er–I distances obtained around the cluster are marginally smaller than those found here for Y–I, appropriate to the slightly smaller radius usually exhibited by the heavier metal,[17] the Er–Er distances in the chain are ≥0.10 Å *larger* than Y–Y separations in Y_4I_5C, and most significantly, the average radius deduced for the postulated interstitial is 0.18 Å *greater* than that shown by carbon in many examples (above). The size seems more appropriate for silicon,[20] although we have not been able to achieve recognizable products following the purposeful introduction of silicon in analogous synthetic reactions. We have noted elsewhere[21] that even Pyrex glass impurities can furnish mixed boron–silicon interstitials in zirconium iodide clusters that are effectively ~0.13 Å larger than carbon.

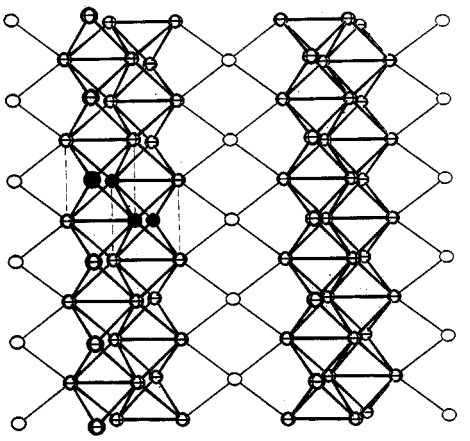

Figure 5. Metal chains in $Y_6I_7C_2$ together with the interconnecting I4 atoms as viewed approximately along the *c* axis. The edge-bridging I1, I2, I3, and the carbon atoms have been omitted for clarity. The repeat distances along and the apex atoms in two shared octahedra are emphasized.

$Y_6I_7C_2$. The cluster chains in this phase represent the result of a further, side-by-side condensation of two Y_4I_5C-like single chains through sharing of Y–Y edges. Every cluster unit contains a single carbon atom, the exposed chain edges are again bridged by iodine, and the exposed metal vertices are likewise bonded either to four-coordinate bridging I4 (at Y3) to form sheets or to an edge-bridging I2 in another cluster (at Y1). A view approximately along $\vec{c}$ of just the bare metal chains plus the four-coordinate iodine that interconnects these into layers is shown in Figure 5. To assist in the visualization, the unshared vertices (Y1) in an adjoining pair of the octahedral building blocks are darkened in the figure, and their elongated edges along *b* (Y2–Y2′, Y3–Y3′) are dashed in.

Shared metal edges between these nominal octahedra (3.33 Å × 2, 3.44 Å) are not as short as in Y_4I_5C, and some further distortion of the octahedra accompanies the edge sharing. Thus the Y2 atoms involved in the additional edge condensation are in effect displaced toward carbon in the adjoining chains (Figure 2). Even so, Y2–C remains long, 2.65 Å, and other Y–C distances range down to 2.36 Å to Y1. (The average Y–C distance is 0.08 Å larger than that found in Y_4I_5C, possibly a reflection of a matrix effect from the iodine or a more complex bonding in this condensation product.) The relative dimensions within the chains in $Y_6I_7C_2$ parallel those within $Sc_7Cl_{10}C_2 = ScCl_3{\cdot}Sc_6Cl_7C_2$[15] remarkably well. We observed earlier that carbon in $Sc_7Cl_{10}C_2$ was generally displaced from the center of the nominal scandium octahedra toward those scandium atoms with fewer metal and more halogen neighbors, i.e., those that are presumably more positive, and the same applies here. (Such is not the case in Y_4I_5C.) As with the Y_4I_5C vs the $ScCl_3{\cdot}Sc_4Cl_5C$ structures (above), the $Y_6I_7C_2$ arrangement can be conceptually converted to the analogue of the $ScCl_3{\cdot}Sc_6Cl_7C_2$ type readily through removal of the I4 bridges, expansion of the structure, and insertion of $ScCl_{4/2}Cl_2$ chains with these halides bonded exo at the equivalent of the Y1 and Y3 vertices.

This basic structure was first reported for the pseudobinary phases Er_6I_7 and Tb_6Br_7.[9] The cell and cluster sizes for each are reasonable for carbides. No electron density residuals were reported. Later, the existence of both $Gd_6Br_7C_2$ and $Gd_6I_7C_2$ with basically the same structural framework was noted without detail.[6]

Physical Properties. The new carbide phases might be expected to exhibit pseudo-one-dimensional properties based on their crystal structures, and yet no physical data are available on any structural analogue save for the semiconducting (and empty) chain phases

(17) Shannon, R. D. *Acta Crystallogr., Sect. A: Cryst. Phys., Diffr., Theor. Gen. Crystallogr.* **1976**, *A32*, 751.
(18) Ziebarth, R. P.; Corbett, J. D., to be submitted for publication.
(19) Hwu, S.-J.; Dudis, D. S.; Corbett, J. D. *Inorg. Chem.* **1987**, *26*, 469.
(20) Smith, J. D.; Corbett, J. D. *J. Am. Chem. Soc.* **1986**, *108*, 1927.
(21) Rosenthal, G.; Corbett, J. D. *Inorg. Chem.* **1988**, *27*, 53.

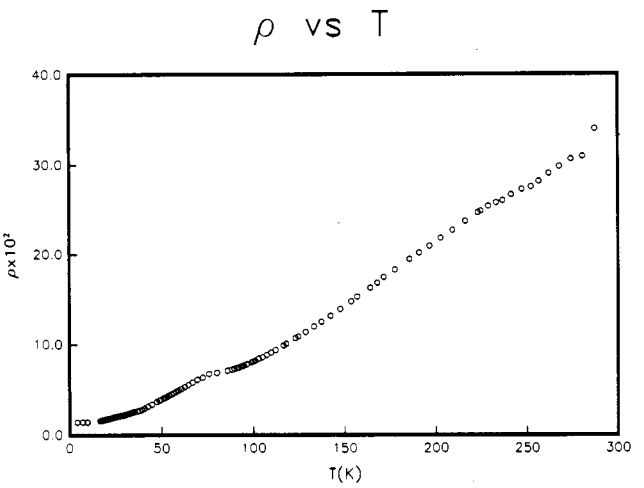

Figure 6. Resistivity (Ω cm × 10^2) of $Y_6I_7C_2$ along the chain axis as a function of temperature (K) according to four-probe ac measurements.

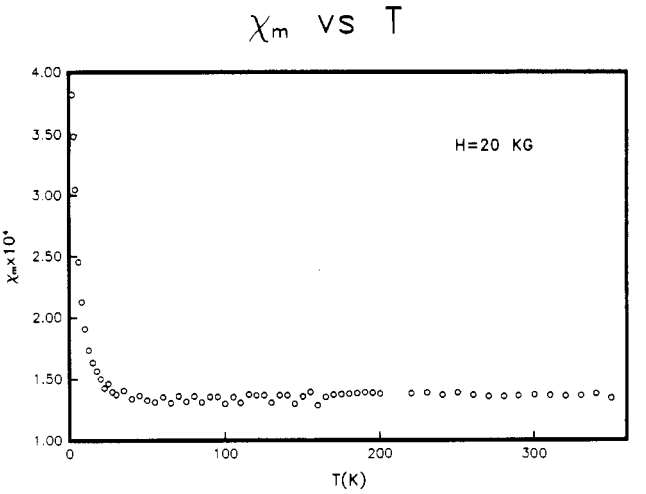

Figure 7. Molar magnetic susceptibility (×10^4) of $Y_6I_7C_2$ as a function of temperature (K) (H = 20 kG).

Gd_2Cl_3 and Tb_2Cl_3,[22,23] both of which are isostructural with Y_2Cl_3 and Y_2Br_3. Y_4I_5C and $Y_6I_7C_2$ each have three electrons per formula unit remaining after the valence orbitals/bands of the nonmetals are filled, and the results of extended Hückel calculations for both (below) are strongly indicative of metallic behavior. Therefore, resistivity and susceptibility measurements were carried out on both phases to clarify their behaviors. The extreme sensitivity of these crystals to surface oxidation thwarted attempts at four-probe resistivity measurements until it was found that pressed indium contacts evidently penetrated the surface well enough to allow good data to be obtained. Large needle crystals of $Y_6I_7C_2$ could also be obtained, making it the prime candidate for measurements. Crystals of Y_4I_5C obtained so far have been too small for the attachment of four leads, but two-probe measurements indicate good conductivity at room temperature.

The resistivity data for $Y_6I_7C_2$ are shown in Figure 6. The slight discontinuity at ~75 K was attributed to the loss of thermal equilibrium between the sample and the thermometer during liquid-helium transfer. The temperature dependence of the data indicates that $Y_6I_7C_2$ has metallic behavior. The room-temperature resistivity (ρ_{298} ~ 0.3 Ω cm) is relatively high for a metal. The values may be significantly higher than the intrinsic value because of macroscopic effects arising from the fibrous nature of the material; in particular, the pressure contacts provided by indium leads (see Experimental Section) may not yield a uniform current flux through the crystal. There is no clear evidence for any distortion of the chains over the temperature range measured (unless it occurs near 75 K). X-ray powder diffraction results obtained at 25 and 293 K are also consistent with the absence of a distortion in this range.

The molar magnetic susceptibility data shown in Figure 7 reveal only a small temperature- and field-independent paramagnetism, consistent with a metallic property and the absence of any evident phase change. The increase in susceptibility at the lowest temperatures is common and is usually associated with traces of paramagnetic impurities. Susceptibility data obtained for Y_4I_5C were not as useful as the samples always contained ~30% $Y_6I_7C_2$ and also small amounts of ferromagnetic impurities (equivalent to ~220 atomic ppm of Fe). However, the absence of an recognizable contributions by Y_4I_5C to this background suggests that only a small paramagnetism is present, roughly comparable to that of $Y_6I_7C_2$.

Electronic Structure and Bonding. Interest in the bonding within the chains and the role of carbon prompted us to perform extended Hückel band structure calculations on both phases. Calculations were performed on one-dimensional-model chains with formulas

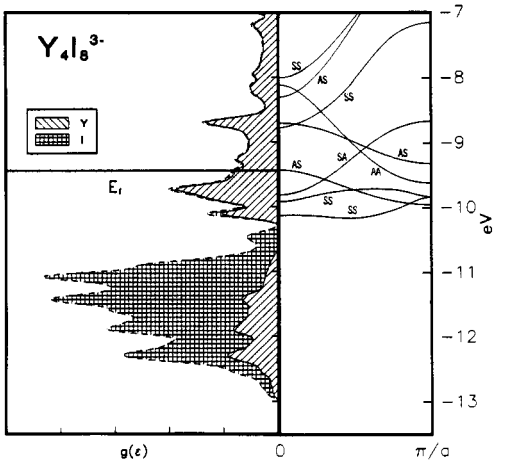

Figure 8. Yttrium band structures and densities of valence states near E_F in Y_4I_5. The metal and iodine contributions to the DOS are shown. The labels SS, AS, and AA refer to symmetry properties of bands contributing to the conduction band (see text).

$Y_4I_8C^{3-}$ and $Y_6I_{10}C_2^{3-}$ as well as on the carbon-free hosts in order to judge the effect and importance of the interstitial. Three additional iodine neighbors beyond the number actually present in the compounds are required in each case in order to properly reflect the yttrium coordination environments, namely the two iodines that are exo to the apex yttrium atoms plus a second edge-bridging iodine bonded in a square-planar manner between chains (Figures 1 and 2). The dangling lone pairs from these iodines add spurious levels to the top of the iodine valence band ~1–2 eV below the Fermi level, but this alteration is unimportant since we are primarily interested in the metal orbitals and metal–carbon interactions. As mentioned earlier, the $Y_4I_8^{3-}$ structure was idealized by use of very slightly altered bond lengths so that the chain contained two normal mirror planes, xy lying in the shared edges and xz containing the vertices of the "octahedra" (Y2) and carbon (Figure 3). Atomic coordinates for $Y_6I_{10}^{3-}$ were taken directly from the refined structural parameters.

In Figures 8 and 9 we show the pertinent band structures in the region of the metal conduction band and the density of states (DOS) plots for $Y_4I_8^{3-}$ and $Y_4I_8C^{3-}$. In both diagrams the dispersion curves are given two-letter labels ordered according to their reflection symmetry in the xy and xz planes, respectively (S = symmetric, A = antisymmetric). We may anticipate that the metal-rich bands for $Y_4I_8^{3-}$ with SS, SA, and AS symmetry will be perturbed by inclusion of the carbon atom since it has four valence orbitals of like symmetry: s and p_x, SS; p_y, SA; p_z, AS.

The "spaghetti" in these figures gives us some direct information on the changes that occur on moving from $Y_4I_8^{3-}$ to $Y_4I_8C^{3-}$. We will focus on bands with predominantly yttrium character (those

(22) Ebbinghaus, G.; Simon, A.; Griffith, A. *Z. Naturforsch., A: Phys., Phys. Chem., Kosmophys.* **1982**, *37A*, 564.
(23) Bauhofer, W.; Simon, A., *Z. Naturforsch. A: Phys., Phys. Chem., Kosmophys.* **1982**, *37A*, 568.

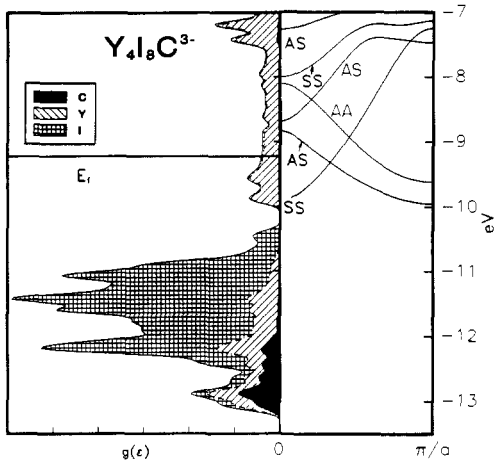

Figure 9. Yttrium band structures and densities of states near E_F in Y_4I_5C with carbon contributions darkened. The labels SS, AS, and AA refer to symmetry properties of bands contributing to the conduction band (see text).

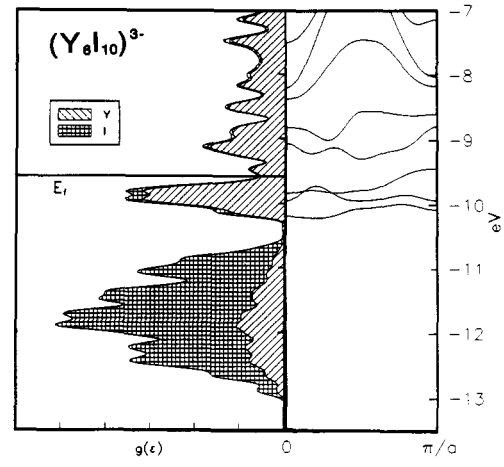

Figure 10. Yttrium band structures and densities of states near E_F in Y_6I_7. Included are the projections of yttrium and iodine contributions to the total DOS.

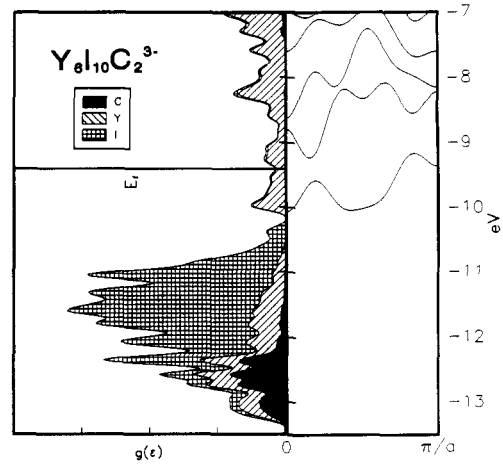

Figure 11. Metal band structures and densities of valence states in Y_6I_7C with carbon contributions darkened.

above −10.3 eV) and take each symmetry type in turn. For $Y_4I_8^{3-}$, there are three bands of SS symmetry, plus part of a fourth, in the yttrium d band region. Two of these bands are wholly below the Fermi level. This situation is altered considerably in $Y_4I_8C^{3-}$ where now there are only two SS bands in the energy window and only about one-third of one of them falls below the Fermi level. Clearly, the lower lying carbon s and p_x "donor" levels have interacted with Y–Y bonding "acceptor" bands and in the process have been pushed up in energy, while two Y–C bonding bands of SS symmetry (not shown) have simultaneously appeared at lower energies. The carbon p_y orbital effectively contributes to a bonding band as well, and the SA band that traverses the Fermi level in $Y_4I_8^{3-}$ disappears from the energy window in $Y_4I_8C^{3-}$. The situation for the AS bands is again similar: there are two bands below ~9 eV in $Y_4I_8^{3-}$ and only one such in $Y_4I_8C^{3-}$; the carbon p_z orbital is of course the culprit. Naturally, the single AA symmetry band is unaltered between the two figures since the carbon center has no orbitals of this symmetry.

To summarize, each of the carbon orbitals finds a symmetry match in the lower reaches of the metal–metal bonding bands of the erstwhile empty chain. The fate of the carbon p bands can be traced by examining the blackened portion of the projected DOS plot in Figure 9. Since the p orbitals of "free" carbon have an H_{ii} (valence state orbital energy) value of −11.4 eV, one can see that they have been considerably stabilized by mixing with the yttrium orbitals. Thus, much of the Y–Y bonding is sacrificed to the Y–C bonding. In the DOS plots, the appearance of the Y–C bonding contribution at ~−13 eV is accompanied by a clear DOS decrease in the portion of the yttrium conduction band shown. Changes in the overlap population (supplementary material) reflect the same effects. A stabilization of the chain structure on inclusion of carbon is evident.

All of the above is quite analogous to the treatments of main-group interstitials encapsulated in isolated clusters presented in previous work.[3,20,24] Particularly notable is the one-to-one correspondence between the disappearance of metal–metal bonding levels and the appearance of metal–interstitial bonding levels in the occupied manifold.

Since double chains in $Y_6I_7C_2$ possess no symmetry elements that pass through the carbon atom sites, the kind of analysis presented for the single-chain system is not possible for the double-chain system. Nevertheless, inspection of Figures 10 and 11 make it quite clear that a similar situation obtains. It should be noted that the two-fold screw axis at ($^1/_4$, y, $^1/_2$) along the double chain enables us to "unfold" the band structure so that each band shown in these figures can hold 2 e/Y_3I_5C unit or 4 e/$Y_6I_{10}C_2$ unit (for an example, see ref 25). Thus, addition of two carbon atoms to Y_6I_{10} adds only four lower lying bands (one s, three p) to the band structure as presented in Figure 11, and we expect that as many metal-rich bands will be pushed up by Y–C interactions and become antibonding. Inspection of both the dispersion curves and the DOS plots shows that, at least qualitatively, this is what happens. Because of the way in which the bands cross the top of our energy window at −7 eV, the precise number of bands "pushed up" is not defined, but it is somewhere between three and four per added carbon atom. Not only are the qualitative changes in the DOS comparable to the situation for the single-chain system but also one may see the same trend in calculations that compare the bonding in ZrCl (i.e., Zr_2Cl_2) with its filled counterpart Zr_2Cl_2C.[26]

Conclusions. Bonding in the infinite-chain phases Y_4I_5 and Y_6I_7 is markedly stabilized by Y–C bonding when interstitial carbon is introduced into all metal octahedra of the hypothetical empty chain. Four low-lying Y–Y d bands overlap with the four carbon oribtals in such a way that the Y–Y bands are raised and four low-lying Y–C bands appear. This can be seen clearly in the DOS illustrations and in the atom contributions to these. Each phase is predicted to have three electrons per formula unit in a broad, metal-based conduction band. The physical data obtained for $Y_6I_7C_2$ are consistent with the extended-Hückel calculations; the compound is a metal over the 10–290 K region measured and exhibits a Pauli-like paramagnetism. Although this phase has a pseudo-one-dimensional structure, no Peierls (or other) distortion is evident down to 15 K. Preliminary data on Y_4I_5C indicate that

(24) Smith, J. D.; Corbett, J. D. *J. Am. Chem. Soc.* **1985**, *107*, 5704.
(25) Hughbanks, T.; Hoffmann, R.; *J. Am. Chem. Soc.* **1983**, *105*, 3528.
(26) Ziebarth, R. P.; Hwu, S.-J.; Corbett, J. D. *J. Am. Chem. Soc.* **1986**, *108*, 2594.

it too has a low resistance at room temperature but other physical data could not be obtained because of experimental difficulties.

Acknowledgment. The principal portions of this research (S.M.K., T.H.) were supported by the National Science Foundation—Solid State Chemistry—under Grant DMR-8318616. The susceptibility and resistivity measurements were carried out within a solid-state physics program supported by the Materials Sciences Division, Office of Basic Energy Sciences, U.S. Department of Energy. All of the research described was carried out in the facilities of Ames Laboratory, DOE. We thank Charles Hewitt for help in obtaining resistivity measurements.

Supplementary Material Available: Tables of anisotropic thermal parameters for Y_4I_5C and $Y_6I_7C_2$, extended Hückel input parameters, and overlap populations (3 pages); tables of observed and calculated structure factors for Y_5I_5C and $Y_6I_2C_2$ (6 pages). Ordering information is given on any current masthead page.

Contribution from the Department of Chemistry,
Colorado State University, Fort Collins, Colorado 80523

Spontaneous and Reversible Interaction of Vanadium(V) Oxyanions with Amine Derivatives

Debbie C. Crans* and Paul K. Shin

Received December 23, 1987

The interaction between vanadate and tri- or tetradentate ethanolamine derivatives has been studied by using ^{51}V NMR spectroscopy. The reactions occur spontaneously in aqueous solutions, at ambient temperatures and in the physiological pH range. In addition to one amine group and one hydroxyl group, the ethanolamine derivative should contain a third and/or fourth functionality that is an alcohol, a carboxylic acid, a phosphonium acid, or an amine. The reactions are highly dependent on pH, concentrations of monomeric vanadate, and amine. The stability constants for the complexes are minimum orders of magnitude greater than those found for vanadate derivatives of corresponding ether derivatives, and the high stability is associated with the central nitrogen. Only one vanadium complex is formed in substantial amounts in the reaction of ethanolamine derivatives with vanadate, and that complex is mononuclear in vanadium. Several of the ethanolamine derivatives that form complexes are commonly used buffers in biological and biomedical studies in vitro.

Introduction

Vanadium is a trace element whose role in biological systems is obscure. Several organisms including sea squirts, mushrooms, algae, chickens, and rats require vanadium as an essential element.[1] Human dietary intake averages 10–60 μg/day, and although vanadium appears beneficial at low levels, high levels of this element are toxic.[1] Vanadate ($H_2VO_4^-$) induces many biological effects, including cardiovascular activity and hormonal action, but little is known about the chemical and biochemical function of vanadium. We now describe chemical reactions that can occur under physiological conditions between vanadate and various amine derivatives. These reactions can lead to serious (and unappreciated) complications when biological studies are conducted in vitro and in vivo with vanadate.

Vanadium(V) has the potential to act as a phosphorus analogue.[2] The three pK_a's of vanadic acid are less than 1 pH unit from the pK_a's of phosphoric acid, and as a result the aqueous acid–base chemistry of vanadate is very similar to that of phosphate.[2] The ability of vanadate to substitute for phosphate in many biological systems demonstrates the similarity between these two ions biologically.[1] In addition to its other similarities to phosphate, vanadate also has the tendency to expand the coordination sphere of vanadium and spontaneously generate oligomers[3,4] or other derivatives.[5,6] These remarkable reactions occur at ambient temperatures in aqueous solutions and in the neutral pH range. Examples include the reactions of monomeric vanadate with oligomers of vanadate,[2-4] the reactions of vanadate with catechols and alcohols,[5] and the reactions of vanadate with phosphate or arsenate.[6] Similar reactions have not previously been reported for ligands with non-oxygen donor atoms; this paper describes such a group of reactions. We furthermore show that at least one non-oxo ligand is essential for the high stability of these vanadium complexes.

A vanadium(V) complex of EDTA has been characterized and studied by X-ray crystallography.[7] Related vanadium complexes of the ligand ethylenebis((*o*-hydroxyphenyl)glycine) have recently been studied.[8] Other derivatives of vanadium(V) containing vanadium–nitrogen bonds have been prepared, and in a few cases structural results are available.[9] A derivative of triethanolamine and vanadium(V) is used as a mild oxidation reagent for specific oxidation of α-ethylenic and α-acetylenic alcohols in organic synthesis.[10,11] In vitro studies of biological systems often use triethanolamine and derivatives as buffers.[1,12,13] It is, therefore, of interest to examine whether vanadium ethanolamine complexes form spontaneously in aqueous solutions.

We now describe the spontaneous production of mononuclear vanadium complexes of ethanolamine derivatives in aqueous solutions as observed by ^{51}V NMR spectroscopy.[3,4] The properties

(1) (a) Nechay, B. R.; Nanninga, L. B.; Nechay, P. S.; Post, R. P.; Grantham, J. J.; Macara, I. G.; Kubena, L. F.; Phillips, T. D.; Nielsen, F. H. *Fed. Proc., Fed. Am. Soc. Exp Biol.* **1986**, *45*, 122. (b) Chasteen, N. D. *Struct. Bonding (Berlin)* **1983**, *53*, 105. (c) Nechay, B. R. *Annu. Rev. Pharmacol. Toxicol.* **1984**, *24*, 501. (d) Kustin, K.; McLeod, G. C.; Gilbert, T. R.; Briggs, L. B. R., 4th *Struct. Bonding (Berlin)* **1983**, *53*, 139.
(2) Pope, M. T.; Dale, B. W. *Q. Rev., Chem. Soc.* **1968**, *22*, 527.
(3) Habayeb, M. A.; Hileman, O. E., Jr. *Can. J. Chem.* **1980**, *58*, 2255.
(4) Heath, E.; Howarth, O. W. *J. Chem. Soc., Dalton Trans.* **1981**, 1105.
(5) (a) Kustin, K.; Liu, S.-T.; Nicolini, C.; Toppen, D. L. *J. Am. Chem. Soc.* **1974**, *96*, 7410. (b) Ferguson, J. H.; Kustin, K. *Inorg. Chem.* **1979**, *18*, 3349. (c) Gresser, M. J.; Tracey, A. S. *J. Am. Chem. Soc.* **1985**, *107*, 4215. (d) Gresser, M. J.; Tracey, A. S. *J. Am. Chem. Soc.* **1986**, *108*, 1935. (e) Tracey, A. S.; Gresser, M. J. *Proc. Natl. Acad. Sci. U.S.A.* **1986**, *83*, 609.
(6) Tracey, A. S.; Gresser, M. J. *J. Am. Chem. Soc.* **1986**, *108*, 6229.
(7) (a) Scheidt, W. R.; Collins, D. M.; Hoard, J. L. *J. Am. Chem. Soc.* **1971**, *93*, 3873. (b) Scheidt, W. R.; Countryman, R.; Hoard, J. L. *J. Am. Chem. Soc.* **1971**, *93*, 3878.
(8) (a) Bonadies, J. A.; Carrano, C. J. *Inorg. Chem.* **1986**, *25*, 4358. (b) Bonadies, J. A.; Carrano, C. J. *J. Am. Chem. Soc.* **1986**, *108*, 4088.
(9) (a) Djordjevic, C.; Craig, S. A.; Sinn, E. *Inorg. Chem.* **1985**, *24*, 1281. (b) Yamada, S.; Katayama, C.; Tanaka, J.; Tanaka, M. *Inorg. Chem.* **1984**, *23*, 253. (c) Szentivanyi, H.; Stomberg, R. *Acta Chem. Scand., Ser. A* **1983**, *A37*, 709. (d) Preuss, F.; Fuchslocher, E.; Sheldrick, W. S. *Z. Naturforsch., B: Anorg. Chem. Org. Chem.* **1985**, *40B*, 363.
(10) Mittal, R. K. *Z. Anorg. Allg. Chem.* **1967**, *351*, 309.
(11) Chabardes, P.; Kuntz, E.; Varagnat, J. *Tetrahedron* **1977**, *33*, 1775.
(12) Perrin, D. D.; Dempsey, B. *Buffers for pH and Metal Ion Control*; Chapman and Hall; New York, 1974.
(13) Good, N. E.; Winget, G. D.; Winter, W.; Connolly, T. N.; Izawa, S.; Singh, R. M. M. *Biochemistry* **1966**, *5*, 467.

0020-1669/88/1327-1797$01.50/0